Use of a New Portable Instrumented Impactor on the NASA Composite Crew Module Damage Tolerance Program

for

Proceedings of the American Society for Composites 29th Conference and 16th US-Japan Conference and ASTM D30 Meeting

Wade C. Jackson
Daniel L. Polis

ABSTRACT

Damage tolerance performance is critical to composite structures because surface impacts at relatively low energies may result in a significant strength loss. For certification, damage tolerance criteria require aerospace vehicles to meet design loads while containing damage at critical locations. Data from standard small coupon testing are difficult to apply to larger more complex structures. Due to the complexity of predicting both the impact damage and the residual properties, damage tolerance is demonstrated primarily by testing. A portable, spring-propelled, impact device was developed which allows the impact damage response to be investigated on large specimens, full-scale components, or entire vehicles. During impact, both the force history and projectile velocity are captured. The device was successfully used to demonstrate the damage tolerance performance of the NASA Composite Crew Module. The impactor was used to impact 18 different design features at impact energies up to 35 J. Detailed examples of these results are presented, showing impact force histories, damage inspection results, and response to loading.

INTRODUCTION

Significant concerns exist regarding the ability of composite structures to meet structural requirements when impact damage is present. In the late 1970s, Rhodes, et al. [1, 2] reported that significant strength loss occurs in carbon-epoxy laminates containing non-visible impact damage. Since that time, extensive research has been conducted on the impact damage response and residual strength. Experimental

Wade C. Jackson, NASA Langley Research Center, MS188E, Hampton, VA 23681, U.S.A.
Daniel L. Polis, Sierra Nevada Corp, Space Systems, 315 CTC Blvd., Louisville, CO 80027, U.S.A.

investigations have primarily focused on small flat coupons where drop-weight test systems are used to inflict damage. ASTM test method D7136 for measuring the impact damage resistance is often used for the impact testing and specifies a 100x150 mm test specimen [3]. Following the impact test, a test for residual compressive strength, such as ASTM test method D7137, can be performed [4]. These compression-after-impact (CAI) tests are often used to generate design allowables [5-7].

In general, results from these coupon tests cannot be directly applied to larger specimens or structures by correlating with impact energy. Small coupons will respond differently than a structure to an impact event. For example, more impact energy will be transferred into the elastic deformation (strain energy) of a larger specimen than a smaller one. Also, the impact response of a larger structure may become very complex if the impact excites structural vibration modes that have periods on the order of the contact duration. In contrast, most small test coupons exhibit a near quasi-static deformation during low-velocity impact [8]. Because impacts produce a complicated three-dimensional damage state (multiple delamination interfaces, intralaminar ply cracking, fiber breakage), impact damage is extremely difficult to predict and model accurately. The impact damage response is a function of the projectile properties (velocity, mass, shape, material, and impact angle) and target properties (material, location, thickness, layup, boundary conditions, geometry, and environmental conditions). Consequently, testing remains the primary means of evaluating the impact damage behavior.

Residual strengths are commonly obtained from small rectangular specimens subjected to uniaxial loading [4]. As with the impact damage response, the coupon residual strength data is also difficult to relate to larger components. Load paths in actual structures are more complex and may involve multi-axial loads (e.g., pressurized structures) and include out-of-plane loads. The effects of geometry and boundary conditions also must be considered. In addition, the residual strength of joints is difficult to determine from small coupon testing.

Following impact testing of structures, the inflicted impact damage can be used to evaluate the damage tolerance using mechanical testing. Most aerospace structures are required to meet specific damage tolerance requirements for certification [5–9]. The structure must be shown, by test or analysis, to have adequate strength when potential damage is present. A Damage Threat Assessment (DTA) must be performed where potential sources of impact damage are identified [5-7, 9, 10]. The threats may occur during fabrication (e.g., tools, assembly equipment, transport equipment), operation (e.g., hail, runway debris, tire blow out, service equipment), or maintenance (e.g., tools, service equipment, ladders). For each threat, the impact energy and resulting damage type, size, and location must be characterized. Depending on the damage type or detectability, the structure may be required to support limit loads, ultimate loads, cyclic loading, or life cycle testing. Damage tolerance criteria also may require that damage at the impact site may not initiate, grow, or have detrimental growth as a result of the loading [5-7, 9, 10].

Commercial impact test systems are designed for small coupon testing and generally consist of a guided weight propelled by gravity. These systems are not suitable for general testing of structures. Consequently, a portable impact device was developed that can be used to impact structural details and larger, more complex specimens. The projectile is propelled using a spring that allows impacts

to be performed at specific locations regardless of angle. The projectile is instrumented to measure force and velocity. Using this device, the impact damage response can be investigated on larger specimens, such as subcomponents, as well as on full-scale vehicles. Specific structural details such as joints and other complex geometries, which cannot be evaluated at the coupon level, can be investigated in-situ. Unlike small coupon tests, tests with the impactor will provide impact response data that accounts for the actual boundary conditions and includes the true transient-dynamic response of the component.

In this report, the construction, features, and operation of a portable impactor are described. The device was used extensively as part of the damage tolerance program of the NASA Composite Crew Module (CCM), which is a full-scale crew module made of carbon-fiber composites [11]. The damage tolerance program was implemented in two phases. In the first phase, the device was used to impact 18 different design features at 8.1 J to simulate low-energy events that may occur during fabrication or maintenance. The effect of higher energy impacts, up to 35 J, was investigated in the second phase. Following each phase, the CCM was subjected to a variety of load cases to evaluate any structural effects of the damage. Detailed examples of these results are presented which show impact force histories, damage inspection results, and response to loading.

PORTABLE IMPACT DEVICE

Description

A device has been developed that propels an instrumented projectile such that it impacts a vehicle, structural component, or other test specimen. The impactor was designed to be portable and easily positioned to impact a specific point on a test article. Except for a breakaway velocity flag, the projectile remains inside a tube during the entire impact for safer operations. The projectile contains a commercial load cell designed to obtain the dynamic force response during the impact event. A two-pronged flag on the projectile passes through an optical detector to obtain the velocity just prior to impact so that the impact energy can be calculated. The device can be hand held or rigidly mounted at any angle such that the impact response can be evaluated at specific positions on a structure.

The primary components of the impact device are an exterior tube, the instrumented projectile, a spring to propel the projectile, a threaded actuator rod, a release pin, a wooden spacer/locator block, and an optical sensor mounted to measure the impact velocity (Figure 1). The tube is aluminum with a length of 88.90 cm and an internal diameter of 5.26 cm. A 26.70 x 1.28 cm slot was machined at one end of the tube to allow the wire for the load cell and the velocity flag to travel along the projectile path. Just prior to impact, the velocity flag passes through an optical gate attached near the exit of the tube. A removable wooden block with a central hole matching the inside diameter of the tube is attached between the aluminum tube and the target. This block is used for alignment purposes and to protect the target from contact by the end of the tube. The block shown in the figure contains a “V” notch to accommodate the geometry of cylindrical test articles. At the opposite end of the tube, a cylinder is attached to the

inside of the tube by four bolts such that the cylinder is flush with the end of the tube. This cylinder contains a threaded central hole that accommodates a threaded 30.5-cm-long actuator rod. The actuator rod contains a fixed nut at the external tip that allows the rod to be screwed into the cylinder to compress the spring. A release pin (not shown) is inserted through a hole in the tube and holds the projectile within the tube while the spring is compressed. To impact the test article, the pin is pulled to release the projectile. Also shown in the figure are two optional aluminum beams that are clamped to the tube. These beams can be clamped to supports such that the tube remains fixed during the impact test.

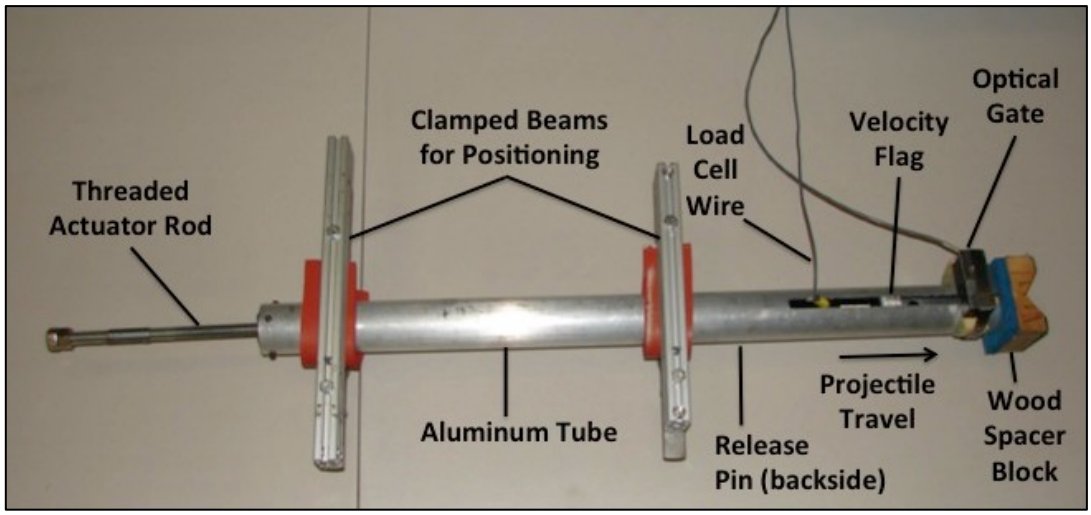

Figure 1. External components of portable impactor.

The internal components of the impactor are shown in Figure 2. The compression block is pushed by the actuator rod and used to compress the spring against the projectile. The block has a conical tip where it contacts the spring in order to keep the spring centered on the block. The spring shown is 88.90 cm long with an outer diameter of 4.76 cm, and has a mass of 0.74 kg. The steel spring has closed ground ends with a manufacturer-specified rate of 5.60 N/mm. Springs can be changed to tailor the impactor to the desired energy range. During operation, the compressed spring propels the projectile to the end of the tube. A release pin passes through a hole in the tube wall and into a slot on the cylindrical mass at the end of the projectile to hold the projectile in place while the spring is compressed. This cylinder has a diameter of 5.08 cm and can be interchanged with pieces having different geometry, length, or material to vary the overall mass of the projectile. The cylinder shown has a mass of 1.00 kg and a length of 7.91 cm. The cylindrical mass is attached to a commercial “impact load cell” that is designed for high-rate loading events. The impact load cell, or tup, is also interchangeable so that the force range can be tailored for the application. The tup shown has a capacity of 22 kN. A cylindrical polytetrafluoroethylene (PTFE) spacer with a central hole is slid onto the end of the tup to maintain alignment within the tube and reduce friction during operation. The PTFE spacer also serves as a mount for the velocity flag.

The velocity flag consists of two metal prongs with 1-cm separation between the prongs' leading edges. The flag is inserted into a slot machined into the PTFE spacer and held in place using an adhesive. An interchangeable impact tip is screwed into the end of the tup. A 2.54-cm-diameter hemispherical tip is shown in Figure 2. The total mass of the current projectile is 1.48 kg.

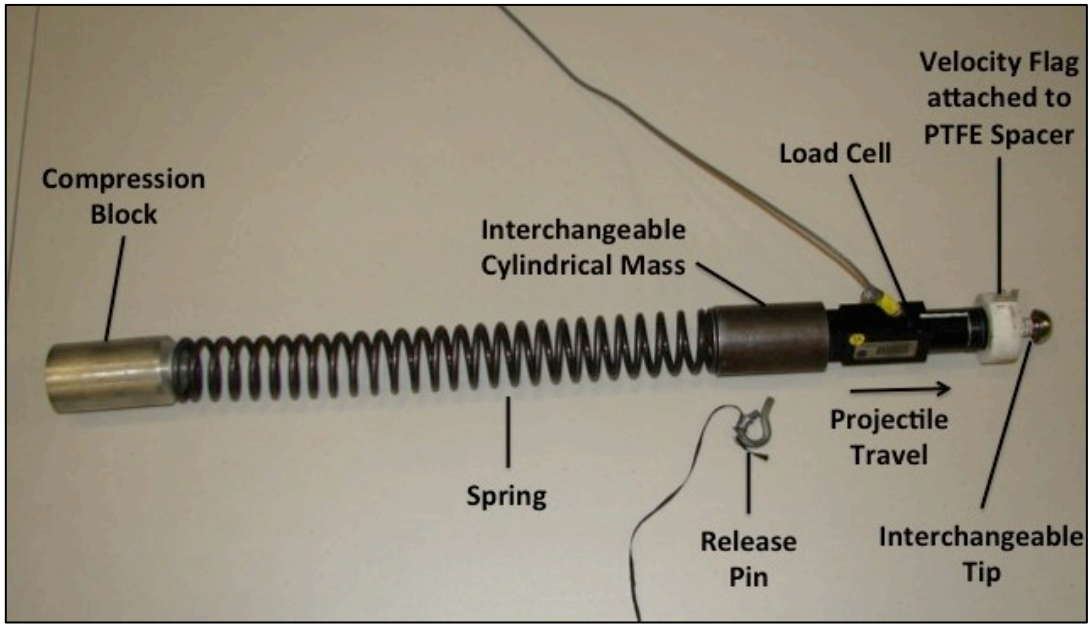

Figure 2. Internal components of portable impactor.

A digital storage oscilloscope is used to record the output from the optical sensor and from the impact load cell. Just prior to contact between the projectile and target, the two-pronged flag passes through the optical sensor, which outputs two pulses that are stored on the oscilloscope. Power and signal conditioning equipment are also required for both the load cell and the optical sensor.

Other than the flag and load cell cable, all the moving parts are contained within the tube so the device is reasonably safe. Both the flag and load cell cable are designed to be separable with direct contact. Under recent testing, this configuration of the portable impactor was used to provide impacts with energies between 4.5 and 35 J. Lower energy impacts are possible with less spring compression. With the current 5.60 N/mm spring, impact energies up to approximately 40 J can be attained. For higher energies, a stiffer spring can be substituted.

Operation

In typical operation, the wooden locator block is first removed from the impactor and centered over the point of interest. An outline of the block is drawn on the target with a marker so that the position can be recreated when the block is attached to the tube. In some cases, the block will need to be modified to conform

to the geometry of a specific target. To maintain alignment during projectile release, the device can be either manually held or clamped to fixed supports using the attached beams. An example of using the clamped beams during an impact test of a large structure is shown in Figure 3. The clamped configuration is preferred to prevent "kickback" during release. The kickback may cause a shift in the intended path of the projectile or a loss in the impact energy. If the clamped configuration is used, the locator block may be omitted by offsetting the tube end slightly from target so that the tube does not contact the target but the projectile remains captured by the tube.

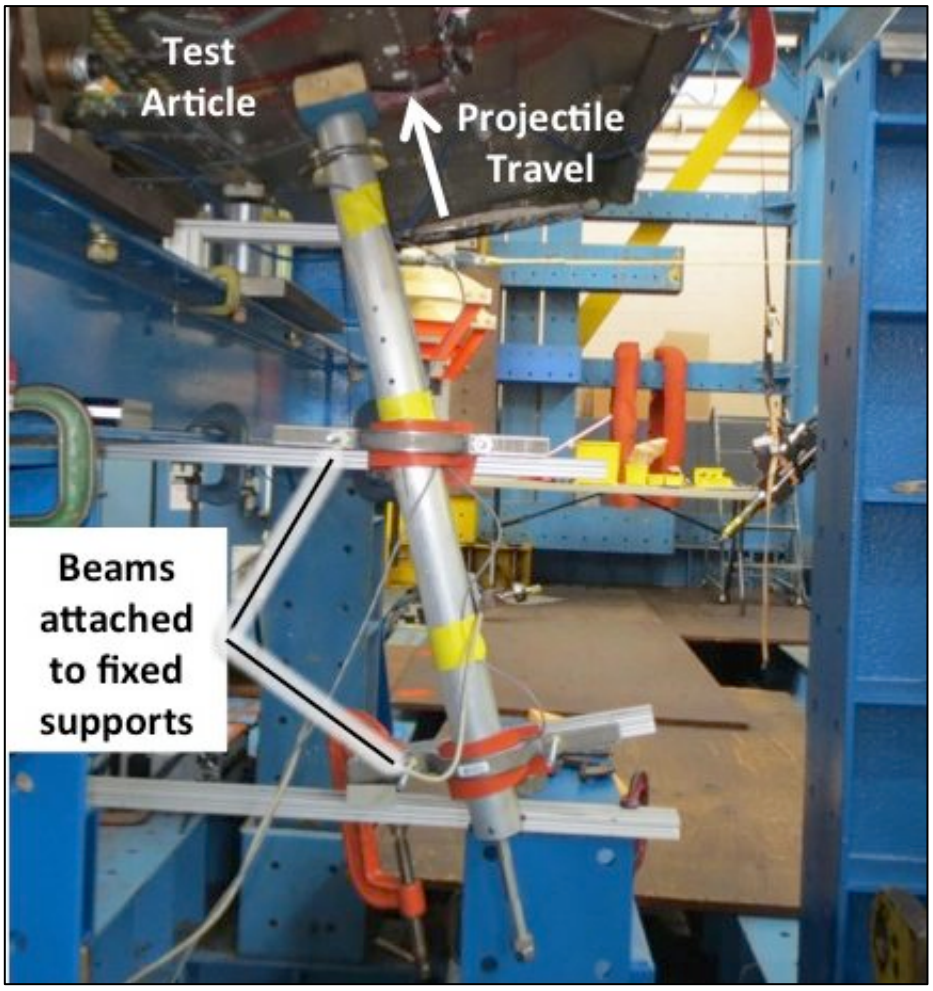

Figure 3. Example of using clamps to position impactor.

The projectile is installed in the tube and held in place by the release pin. The wooden locator block is then attached to the end of the tube. The threaded actuator rod is adjusted until the spring, compression block, and projectile just begin to make contact. This "neutral" position of the actuator rod is then measured and recorded. As the threaded rod is turned with a wrench, the rod presses on the compression block, which compresses the spring against the end of the projectile.

The axial displacement of the actuator rod from the neutral position corresponds to the amount of spring compression and, hence, the energy stored in the spring. At this point, the portable impact device is "armed" and ready to be released. The impactor is manually pressed against the target or clamped into position. The tube must be positioned normal to the target surface to prevent the projectile from binding against the inside of the tube at impact. If a clamped configuration is used, the spring can be compressed after the tube is fixed in place. After the digital storage oscilloscope is set to trigger and record, the release pin is pulled to launch the projectile at the target. For hand-held operation, two people are required: one to position and hold the tube, and one to pull the release pin. If the impactor is clamped into position, the projectile can be remotely released by sharply pulling on a cord attached to the release pin.

The manufacturer of the spring used in the impactor lists a spring constant, k, of 5.60 N/mm. The spring constant during unloading was measured in the lab in order to verify the vendor's value. The force-displacement response was measured over a displacement range of 9.74 cm. The spring response was linear with a constant of 5.74 N/mm. This value was used to calculate the amount of spring compression for the desired impact energy.

The energy stored in the spring is transferred primarily to the projectile. However, some energy is lost due to friction between the projectile and the tube and between the spring and tube. In addition to the frictional losses, the change in potential energy of both the projectile and the spring need to be considered. Recoil of the tube as the projectile is released can also affect the impact energy of the projectile. The amount of spring compression x, was calculated for a target impact energy, E, using Equation 1:

$$x \approx \sqrt{\frac{2\left[E + \left(a\, m_{projectile} + \left(a - \frac{1}{2}x\right) m_{spring}\right) g\, a \sin\alpha\right]}{k}} \qquad (1)$$

where $m_{\text{projectile}}$ is the mass of the projectile, m_{spring} is the mass of the spring, g is the acceleration of gravity, a is the distance the projectile travels prior to impact, α is the inclination angle of the impact tube relative to the horizontal, and k is the spring constant discussed earlier. The inclination angle, α, will be positive if the projectile travels against gravity (upwards) to contact the target and negative if projectile travels with gravity (downwards). Again, Equation 1 assumes friction is negligible. The equation is approximate since it does not account for the spring's kinetic and vibrational energy at the time of impact. The spring compression, x, will need to be calculated for each inclination angle and corresponds to the axial travel that the actuator rod needs to be adjusted relative to the neutral position. Since the projectile position is fixed within the tube for all impact energies, the value of a will not change and only needs to be determined once. Since the spring compression, x, appears on both sides of Equation 2, an iterative procedure was used for the calculation where the initial value of x was calculated by assuming that the spring mass was zero.

Following the impact, the recorded outputs from the load cell and optical sensor are downloaded from the digital storage oscilloscope. Using the force calibration data, voltage output from the load cell is converted to the force history. (Prior to

impact testing, a static calibration is performed with the load cell mounted in a servohydraulic load frame.) The velocity of the projectile at impact, V_i, is calculated based on Equation 2:

$$V_i = \frac{d}{t_2 - t_1} + \left(t_i - \frac{(t_2 + t_1)}{2}\right) g sin\alpha \quad (2)$$

where d is the distance between the leading edges of the two prongs, t_1 and t_2 are the time of each prong's pulse, t_i is the time at impact, g is the acceleration of gravity, and α is the angle of the tube from horizontal. The impact energy is then calculated from this velocity along with the projectile mass. To account for effects not included in Equation 1, the relationship between x, α, and impact energy can be determined experimentally based on the measured projectile velocity.

A variation on this original impactor design, which resulted in a shorter overall length of the device, was created for operations in more confined spaces. With this modified design, the actuator rod was omitted. The spring was compressed by manually pushing the projectile into the tube at the tip and then inserting the release pin at the desired spring compression length, x. This alternate design requires a new hole to be drilled into the tube for each value of x, which also results in a new value of a for each hole. In addition, obtaining precise values of x is difficult using the drilled hole. For higher energy impacts, it may be difficult to manually compress the spring with this design variation.

Note that secondary impacts are possible with this impact device. However, the impact energy associated with secondary impacts will be small compared to the original impact. For safety reasons, this portable impactor was designed to keep the primary moving parts contained in the tube during operation. However, the energy in the compressed spring must be treated with appropriate precautions. When the spring is compressed or being compressed, the front and rear of the impact device must be clear of any personnel.

DAMAGE TOLERANCE TESING ON COMPOSITE CREW MODULE

Overview

The Composite Crew Module (CCM) was a NASA development program funded by the NASA Engineering and Safety Center (NESC) [11]. The program goal was to design, analyze, and manufacture a composite pressure shell, similar in geometry to that of the Orion Crew Module configuration. The final design showing the design features and interface fittings is shown in Figure 4. The CCM is primarily composed of honeycomb sandwich construction with carbon-fiber composite facesheets. It was manufactured in two halves and joined together using an out-of-autoclave splice joint. An aluminum ring was bonded into the docking tunnel to represent the interface to a Low Impact Docking System (LIDS). Six gussets were used that connect the tunnel, ceiling, and LIDS ring. The conic section has cutouts for the hatch and windows. The "backbone" is a grid-like structure that was attached inside the barrel sections. Metallic fittings were used for load introduction for the parachutes and Service Module/Alternate Launch Abort

System (SM/ALAS). Following the manufacture of the CCM, an extensive test program was conducted in order to verify the integrity of the structure and correlate the analysis to the experimental results. The primary testing consisted of internal pressure testing and a series of static point loads while pressurized.

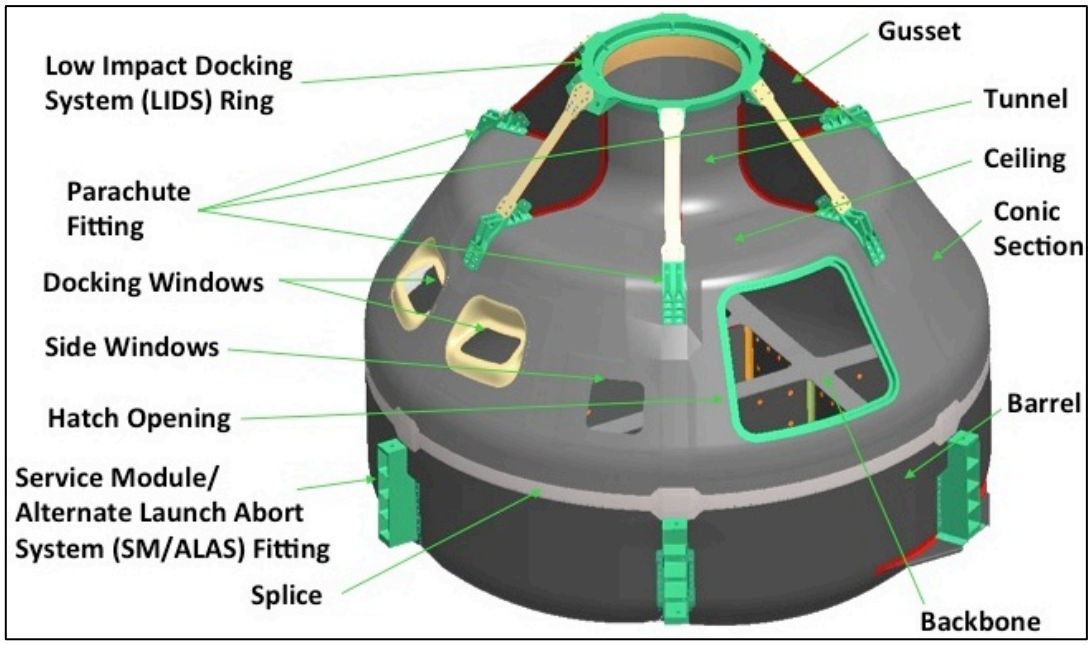

Figure 4. NASA Composite Crew Module (CCM) design.

At the end of this test series, a full-scale damage-tolerance program was developed to demonstrate that the CCM could meet the intent of current NASA requirements [10]. Damage tolerance was included in the design primarily through the use of damage tolerant material allowables. Although the joints were designed to have excess capability, the damage tolerance was still a concern. The CCM damage tolerance program consisted of two phases. In the first phase, the effects of 8.1-J impacts, defined as the allowable threat level, were investigated at 18 unique locations. Following this impact series, the test article was taken through two critical design ultimate load cases followed by life cycle testing. In the second phase, five design details were impacted at critical threat levels, defined as reliably detectable or with a maximum energy of 35.2 J. Following these impacts, life cycle testing was repeated followed by a pressure test to failure. The objectives of the damage-tolerance program were to show that no structural failures occurred and that no damage growth or detrimental damage growth (depending on the test) occurred as a result of the loading. An additional goal was to document the damage size and features as a result of the impact.

To proceed with the impact program, an instrument was needed to apply an impact at a precise location with a specified energy. Impacts were required both internally and externally in the CCM. Highly loaded areas as well as design details such as flanges, joints, and discontinuities were of interest. An impactor that was instrumented to measure force was also desired. By comparing force histories of

similar impacts, test anomalies can be identified. The force history also can show a sudden drop in force that may indicate damage development. Since no commercial impactor meeting these requirements existed, a new instrument was developed for the CCM test program. The end product of this development was described in the previous section. At the time of this investigation, the portable impactor was not instrumented with a velocity detector. Consequently, the impact energies for this program were calculated using Equation 1 instead of directly measured.

All impacts were conducted using a 2.54-cm-diameter hemispherical tip. Prior to each impact, the location was inspected visually and by nondestructive evaluation (NDE) methods such as flash thermography or ultrasound. Following the impact, each location was re-inspected using the same techniques. In addition, the dent depth, if any, was measured and recorded. After each load test, the impact sites were inspected again to determine if any damage growth occurred.

In the first phase, the impact damage response of 18 different design features was investigated using 8.1-J impacts. Impacts at this energy level represented credible threats that may occur during manufacture, transport, maintenance, or operation of the CCM. In Reference 6, the 8.1-J impact level was determined to be a "medium threat" (medium probability) for areas exposed to both operational and maintenance damage. In addition, this type of lower-energy impact has a higher probability of going unreported and/or leaving no visible damage. Examples of some of the CCM impact locations are shown in Figure 5 and are primarily focused on discontinuities (e.g., core ramps – Figure 5c, ply terminations – Figure 5a) and joints (e.g., splice joints – Figure 5b, adhesive joints – Figure 5a, joint flanges – Figure 5d).

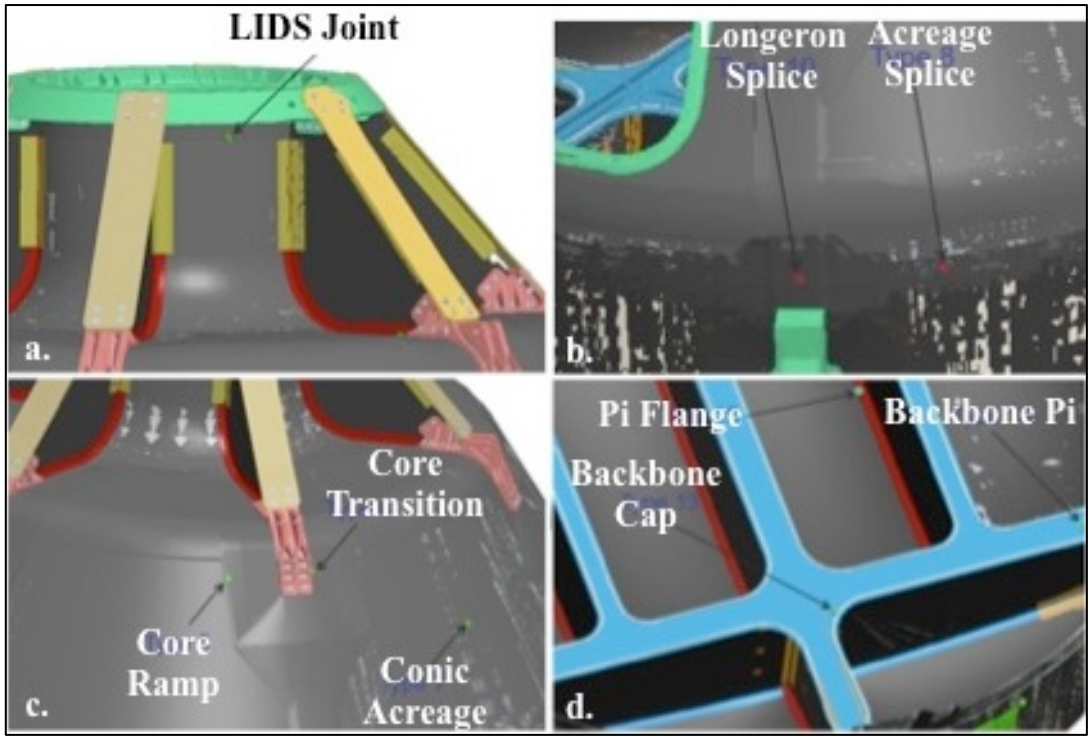

Figure 5. Example of impact locations on a. tunnel,

b. splice joint, c. conic section, and d. internal backbone

Following these impacts, two tests to ultimate load were performed: internal pressure and a mechanical load applied to the main parachute fitting. All impact sites were inspected before and following each test to monitor the damage state. Cyclic testing was then performed that approximated one lifetime of service. The cyclic loading for each lifetime included both mechanical load cycling with internal pressure and internal pressure cycling alone. All 18 impact sites were then reinspected to assess the damage state. Cyclic loading was continued for an additional three life times, and the impact sites were inspected again. The goals in this first phase were to demonstrate structural integrity of the CCM with the impact damage and to demonstrate that no significant growth of the impact damage occurred as a result of the loading and life cycle testing.

For the second phase, seven critical location types were selected from the 18 types used in the first phase. The location types included the Low Impact Docking System (LIDS) adhesive joint (Figure 5a), the acreage in the conic section (Figure 5c), the backbone to shell joint, the backbone cap (Figure 5d), and the splice joint (Figure 5b). The impact damage goal was to create damage states that could be reliably detected visually or through the use of NDE (flash thermography or ultrasonic inspection). For each location type, the impact energy was incrementally increased from 13.6 to 20.3, 27.1, and 35.3 J. A new location was used for each impact, but the site type was kept the same. NDE was used before and immediately after each impact. The impact sequence was stopped when either the damage was readily visible (dent equal to or greater than 0.81 mm), readily detectable by NDE (diameter equal to or greater than 1.3 cm) or a maximum energy of 35.2 J was reached. Following the impacts, cyclic loading, identical to the first phase of testing, was performed to simulate four life times. The impact sites were inspected following the first lifetime and after the fourth lifetime.

The final full-scale test was an internal pressure test to failure. To limit the amount of damage at failure, water was used instead of air to pressurize the test article. Although the final test to failure had many objectives, the damage tolerance objective was to demonstrate the structural capability with a range of impact damage sizes, types, and locations.

During loading, displacement fields around areas of interest, such as impact damage, were obtained using an optical technique called Digital Image Correlation (DIC) [12]. Strain fields were then generated from the displacement fields. Speckle patterns were applied to the CCM around areas where full-field data were desired. A two-camera DIC system was used to obtain a three-dimensional displacement field during deformation. The software optically tracks the position in three-dimensional space of small subsets of the speckle pattern and automatically calculates (differentiation) the strain fields (Lagrangian strain tensor). The DIC data were used to investigate the effects of the impact damage on the structural response. During loading, the strain field around an impact site was monitored in real time from the control room. A more in-depth analysis was performed later on the post-processed data. This DIC technique is well suited for areas with non-uniform geometry and complex loading where strain gages would be unable to capture the complete response. The strain field from a previous analysis was also directly compared to the fields obtained from DIC to validate the analysis. The

areas of interest ranged in size from the entire lobed surface of the barrel (274-cm diameter) to the area around an impact (11 x 17 cm rectangle).

Results

For the first phase of 8.1-J impacts, all 18 impacts were completed as planned. After ultrasonic or thermographic inspection, damage was detected in six of the impact locations. The largest damage was in the conic section, which consists of sandwich structure composed of thin facesheets on a lightweight core. This construction was known to damage easily (due to the lightweight core) and the impact was easily detected visually. The impact resulted in a 0.56-mm dent with a damage size, measured using thermography, of 13 x 11 mm (Figure 6). A region around this impact was speckled and then monitored while the CCM was tested to ultimate pressure (Figure 7). Two images are shown from the DIC that were captured at ultimate pressure. The deformation at the dent is highlighted in the lower left image, and the principal strains are shown in the image on the right. The principal strains are observed to increase around the impact dent. The ply overlaps can be seen on the two images and show somewhat lower strains as expected. The impact damage area was reinspected after loading and no change in damage state was detected.

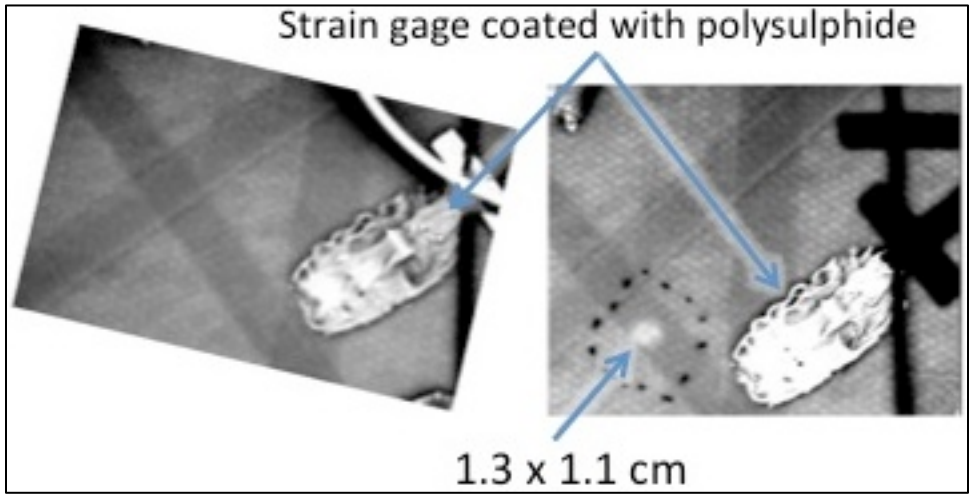

Figure 6. Thermography images of pre (left) and post (right) impact of the conic section.

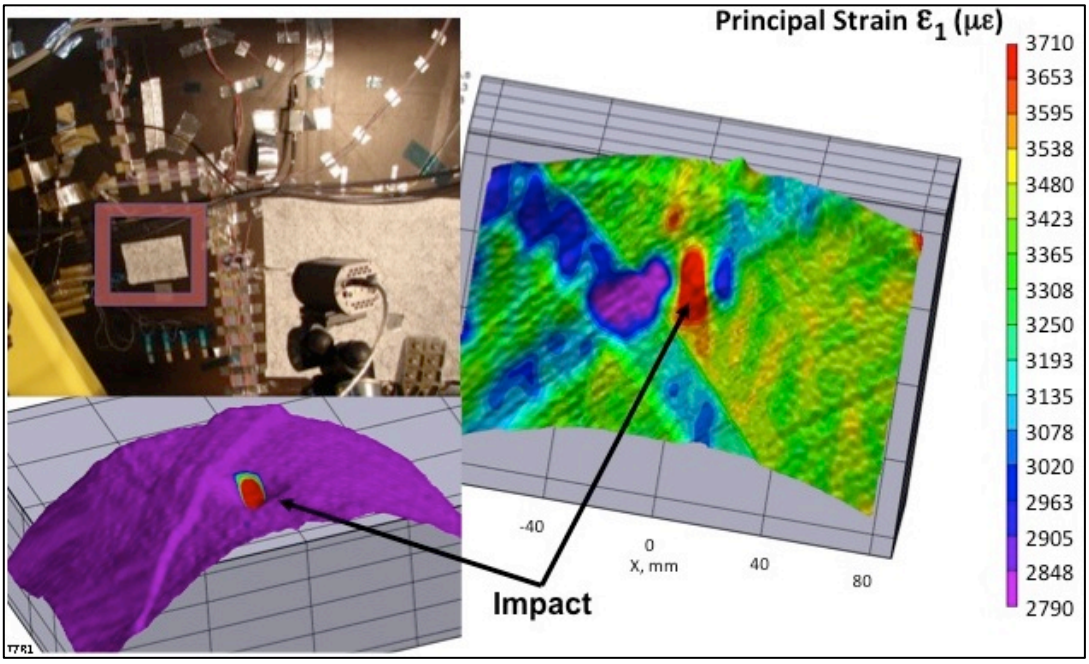

Figure 7. Full-field strain (top right) and deformation (bottom left) for conic section impact during internal pressure to ultimate load.

Impacts at 8.1 J were conducted at two locations near the parachute fitting: the core ramp and near the sandwich-to-laminate transition (Figure 5c). The force histories of these two impacts are shown in Figure 8. Due to the higher out-of-plane stiffness of the impact near the solid laminate, this impact has both a higher peak force and shorter contact duration than the impact at the core ramp. The force history of the core ramp impact shows a sudden drop at the peak force. This behavior is generally associated with unstable damage growth that results in a sudden loss of out-of-plane stiffness. The impact force is larger for the impact near the solid laminate due to the higher out-of-plane stiffness. Both the force histories contain oscillations due to vibrations in the impactor and/or the CCM. As suggested from the force histories, the impact at the core ramp resulted in impact damage while the other impact site showed no damage. Flash thermography showed the damage size was 0.9 x 1.3 cm (Figure 9). However, the impact damage was not visible, and no dent could be detected manually or with a depth gage. Following these impacts, the region around the parachute fitting was speckled so that the structural response could be obtained as the parachute fitting was loaded to ultimate. As shown in Figure 10, no effects of the impact damage were observed in the strain field as a result of the damage. The irregular shaped region for the strain field reflects areas where strains were not computed because of strain gages and wires on the surface. The strain field around the impact near the solid laminate also showed no anomalies. After this load case to ultimate, these impact sites were inspected again and found to be unchanged from previous inspections.

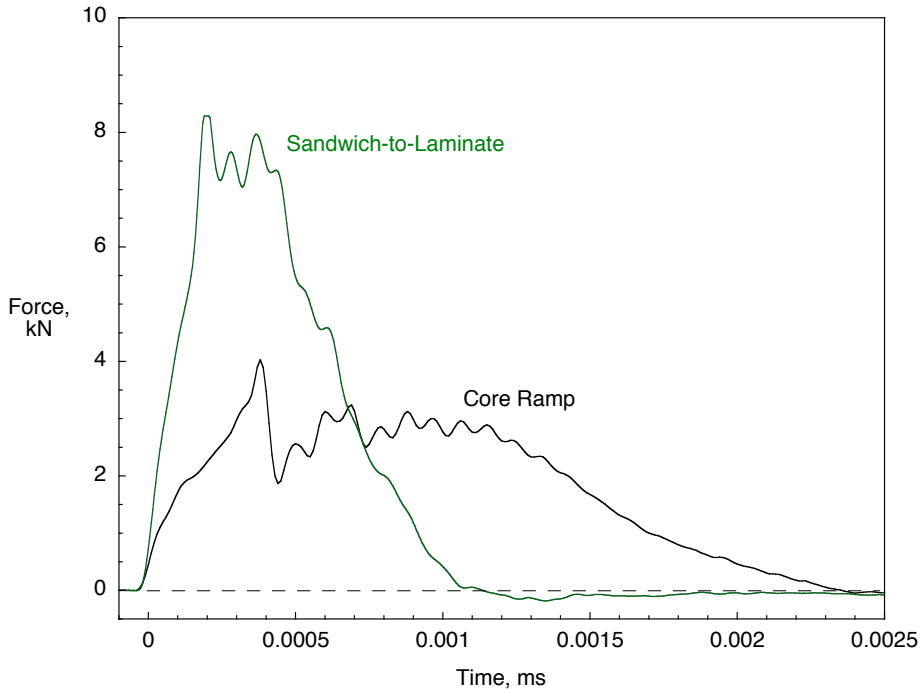

Figure 8. Force histories for 8.1-J impacts of core ramp and sandwich-to-laminate transition area near parachute fitting.

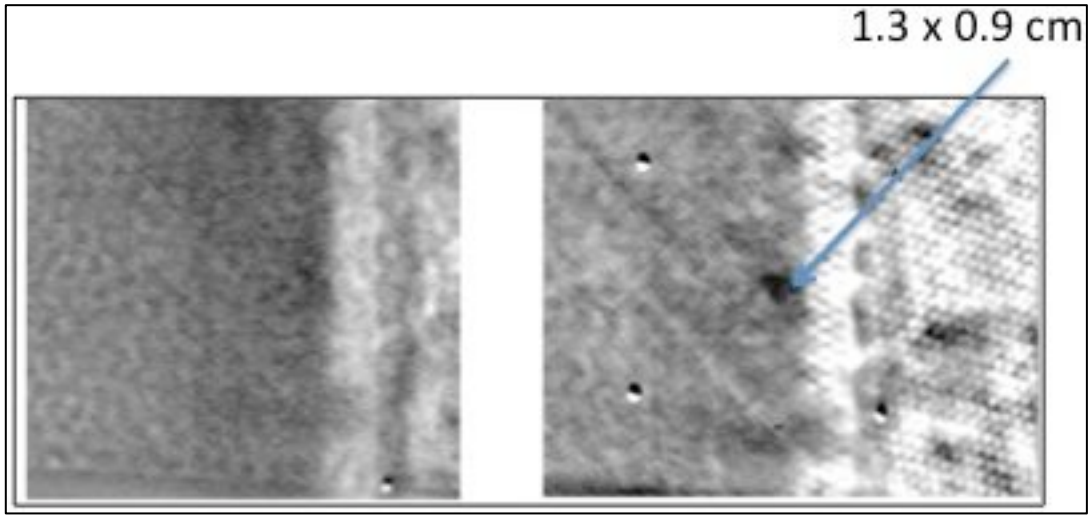

Figure 9. Thermography images for core ramp impact near parachute fitting: pre (left) and post (right)

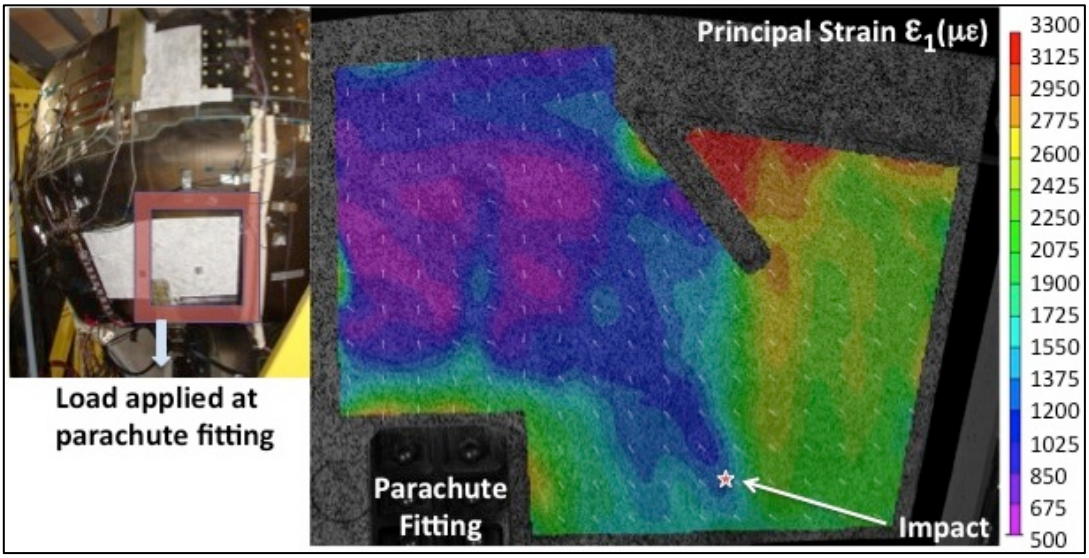

Figure 10. Full-field strain response for the parachute test to ultimate load after 8.1-J impact.

Life cycle testing was conducted following the static testing. After the first and fourth lifetimes were completed, all 18 impact sites were reinspected. For all inspections, no damage initiation or propagation was found. In this phase, the impact damage did not have any adverse effect on the structural performance.

In the second phase of impacts, selected location types were impacted incrementally until a damage threshold or a maximum impact energy was reached. For location types that required impacts with increasing energies, similar sites were selected from around the circumference of the vehicle such that each location received only a single impact. Of the seven critical location types, four received incremental impacts until the maximum energy of 35.3 J was reached. Of these four, one type (longeron splice joint, Figure 5b) had no detectable damage, two types (backbone cap and backbone joint, Figure 5d) had damage sizes below the 1.3-cm diameter threshold, and one type (LIDS joint, Figure 5a) had damage that far exceeded the damage threshold.

As an example, the results of the LIDS joint impacts (Figure 5a), which received four impacts up to the maximum energy, are presented. The force histories are shown for the four increasing impact energies (Figure 11). The first three impacts did not result in detectable impact damage. The 13.6 and 27.1-J impacts have nearly identical contact durations, which indicates that the out-of-plane stiffnesses and hence locations were very similar. However, the 20.3-J impact had a higher peak force and shorter contact duration than the 27.1-J impact, which may indicate that this impact occurred on the internal metallic flange of the LIDS ring instead of at the tip. The impact at 35.3 J had a lower peak force than expected and a longer contact duration, which indicates a loss of out-of-plane stiffness. The force history also contains a sudden drop. Inspection of the impact site showed that the doubler on the inside of the tunnel was debonded over a 5.3 x 8.9 cm region. Both flash thermography and ultrasonic inspections were able to easily detect the damage (Figure 12).

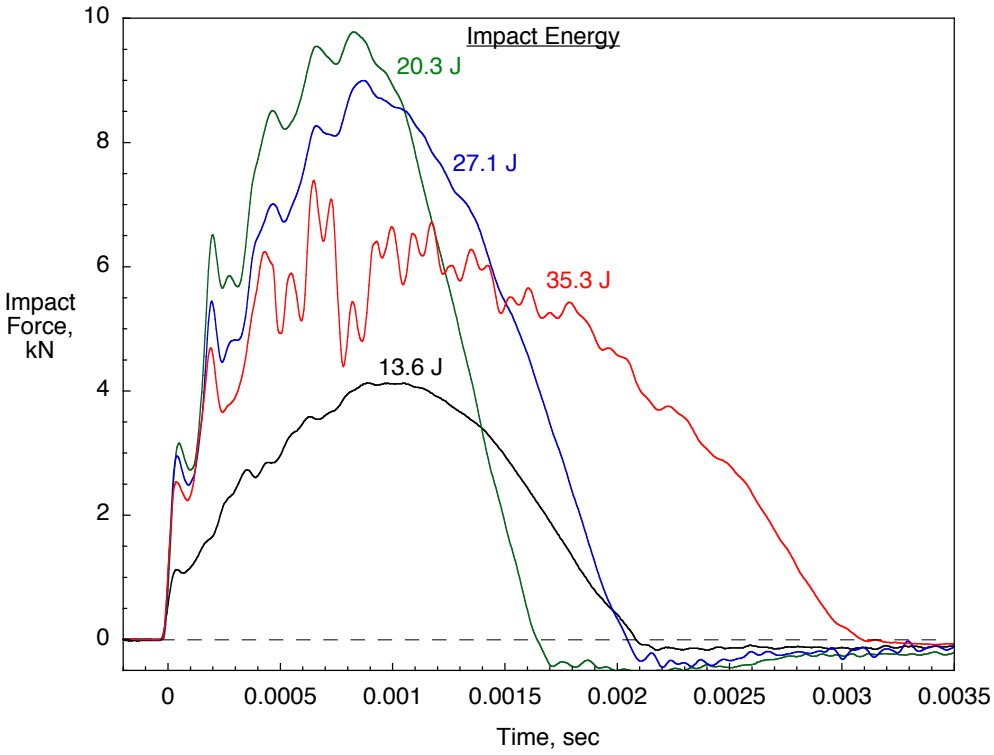

Figure 11. Force Histories for LIDS Joint Impacts

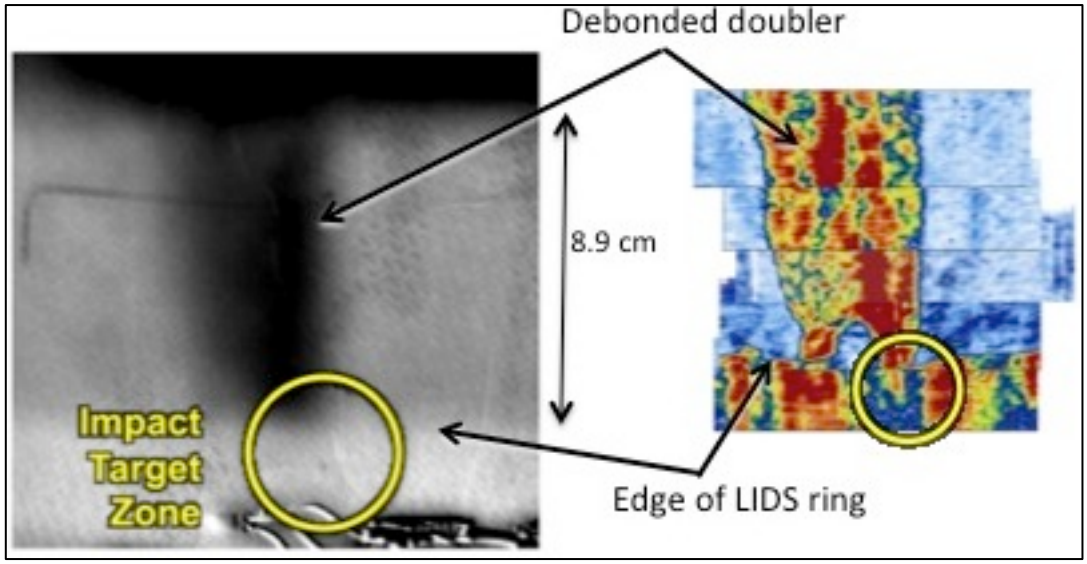

Figure 12. Damage in the LIDS joint from a 35.3-J impact: thermography (left) and ultrasonic (right)

As in the first phase, life cycle testing was performed on the CCM for the equivalent of four life times. Inspections were performed after the first and fourth life times. No significant changes in the impact damage dimensions were measured as a result of the cyclic loading. The CCM was then pressurized hydrostatically

until a significant failure occurred that resulted in a drop in internal pressure. A failure occurred at 175% of ultimate pressure which was caused by core debonds in the transition area between the ceiling and conic sections. All impact sites were reinspected following the test to failure, and no significant impact damage growth or damage initiation was found.

The portable impactor performed extremely well, which allowed the CCM program to meet the damage tolerance testing goals. The two biggest concerns with the impactor were relying on calculated (theoretical) impact energies and imprecise targeting. The effect of friction and other energy losses may result in impact energies that were unacceptably below the desired value as calculated using Equation 1. The kick back during projectile release occasionally resulted in an impact location that was offset from target location. Following the CCM program, two improvements were made to the impactor to address these concerns. A means to measure projectile velocity detector was developed as described earlier. Clamped beams were also added that allowed the impactor to be easily attached to fixed structure during operation. A subsequent test program was used to evaluate these two improvements. The velocity measurement system performed as designed allowing actual impact energy to be calculated. The clamped beams kept the impactor in position, which allowed more precise targeting, and remote operation. Due to the difference in diameters between the projectile and the inside of the tube, the maximum error between actual and desired impact position was approximately 2 mm.

CONCLUDING REMARKS

A new portable impact system was developed that can apply controlled impacts to particular features of test articles. The device is instrumented to record the impact force and the velocity at impact, which allows the impact energy to be calculated. Since the impactor is spring propelled and does not rely on gravity, the device can be positioned at any angle so that the impact damage resistance of specific details can be investigated. For safety purposes, the primary moving parts are all contained within an aluminum tube during operation. In addition, the impact system can be clamped into position and operated remotely, which would be required on loaded test articles. The instrument was originally designed to support the damage tolerance program on the NASA Composite Crew Module (CCM). In the two phases of the CCM damage tolerance program, 36 impacts were successfully delivered to the full-scale test article. Impacts were primarily targeted towards joints and were performed at energies between 8.1 and 35.3 J. The impact response and resulting damage varied greatly depending on the impact energy, geometry, location of boundaries, material thickness, and type of structure. In many cases, features of the impact force history provided indications of the onset of damage. Following the impacts, damage tolerance testing consisted of design ultimate and cyclic life loadings. At the end of the program, the CCM, with all the impact damage present, was loaded to failure using hydrostatic internal pressure. The impact sites were inspected using flash thermography and/or ultrasonic inspection before and after every load case. Most of the impact damage produced was relatively small (less than 2 cm in length). No significant damage growth or

damage initiation was detected during the testing, including the test to failure that reached 175% of ultimate pressure. The portable impact device provided a convenient method for meeting the goals of the CCM program. With the use of this device, it was demonstrated that the CCM could meet the intent of current NASA damage tolerance requirements.

REFERENCES

1. Rhodes, M. D., J. G. Williams, and J. H. Starnes, Jr. 1997. "Effect of Low-Velocity Impact Damage on the Compressive Strength of Graphite-Epoxy Hat-Stiffened Panels," NASA Technical Note, NASA TN D-8411.

2. Rhodes, M. D. 1978. "Impact Tests on Fibrous Composite Sandwich Structures," NASA Technical Memorandum, NASA TM 78719.

3. ASTM D7136/D7136M-12. 2013. "Standard Test Method for Measuring the Damage Resistance of a Fiber-Reinforced Polymer Matrix Composite to a Drop-Weight Impact Event," ASTM International, West Conshohocken, PA.

4. ASTM D7137/D7137M-12. 2013. "Standard Test Method for Compressive Residual Strength Properties of Damaged Polymer Matrix Composite Plates," ASTM International, West Conshohocken, PA.

5. "Certification of Normal Category Rotorcraft." 2008. AC No: 27-1B, Federal Aviation Administration, Washington, D.C.

6. Kan, H. P., R. Cordero, and R. S. Whitehead. 1997. "Advanced Certification Methodology for Composite Structures," DOT/FAA/AR-96/111, Office of Aviation Research, Washington, D.C.

7. Rouchon, J. 2009. "Fatigue and Damage Tolerance Evaluation of Structures: The Composite Materials Response," NLR-TP-2009-221, National Aerospace Laboratory NLR, Amsterdam, The Netherlands.

8. Jackson, W. C., and C. C. Poe, Jr. 1993. "The Use of Impact Force as a Scale Parameter for the Impact Response of Composite Laminates," *J. of Comp. Tech. & Res.*, 15(4):282-289.

9. "Composite Aircraft Structure." 2010. AC No: 20-107B, Federal Aviation Administration, Washington, D.C.

10. "Fracture Control Requirements for Composite and Bonded Vehicle and Payload Structures." 2006. MSFC-RQMT-3479, NASA Marshall Space Flight Center, Alabama.

11. Kirsch, Michael T. 2011. "Composite Crew Module: Primary Structure," NASA/TM-2011-217185, NESC- RP-06-019.

12. Sutton, M. A., J. J. Orteu, and H. Schreier. 2009. *Image Correlation for Shape, Motion and Deformation Measurements: Basic Concepts, Theory and Applications*. Springer, New York.